

Review

Neutron Reflectometry for Studying Corrosion and Corrosion Inhibition

Mary H. Wood [†] and Stuart M. Clarke ^{*} 

BP Institute and Department of Chemistry, University of Cambridge, Cambridge CB2 1EW, UK; maryhwood@gmail.com

^{*} Correspondence: stuart@bpi.cam.ac.uk; Tel.: +44-1223-765700

[†] Current address: Department of Chemistry, University of Birmingham, Birmingham B15 2TT, UK.

Received: 20 July 2017; Accepted: 2 August 2017; Published: 8 August 2017

Abstract: Neutron reflectometry is an extremely powerful technique to monitor chemical and morphological changes at interfaces at the angstrom-level. Its ability to characterise metal, oxide and organic layers simultaneously or separately and in situ makes it an excellent tool for fundamental studies of corrosion and particularly adsorbed corrosion inhibitors. However, apart from a small body of key studies, it has yet to be fully exploited in this area. We present here an outline of the experimental method with particular focus on its application to the study of corrosive systems. This is illustrated with recent examples from the literature addressing corrosion, inhibition and related phenomena.

Keywords: neutron reflectometry; corrosion; corrosion inhibition; adsorption

1. Introduction

The extensive costs of corrosion are well documented, with around 3–4% of the GDP of industrialised countries spent dealing with its effects [1,2]. There exist many excellent texts covering the basics of corrosion [3]; briefly, it is defined as the oxidative degradation of materials, mainly the dissolution of metals and often reprecipitation of corrosive products at the surface. It can be uniform or localised (e.g., pitting), each of which raise different issues for both industrial engineers and scientists studying the phenomena.

The corrosion process can be extremely complex and typically involves numerous inorganic phases such as oxides, hydroxides and a range of corrosion products forming thin films on the metal surfaces. This complexity makes the fundamental study of these systems extremely challenging. However, many of the key aspects of a corroding system can be addressed in situ using neutron reflectometry (NR), such as the dependence of film composition, thickness and roughness on time or as a function of different external environments and the ingress of fluids into the films.

Whilst the formation of passive oxides can protect against further corrosion for some metals in milder environments, inhibitors of various kinds, organic or inorganic, are often added to bind to the metal surface and halt its dissolution. These function by polarising either the cathodic or anodic areas on the surface, or both, to decrease the current density [4]. Organic surfactants are usually classed as mixed inhibitors as they slow both anodic and cathodic reaction rates via adsorption, which blocks both types of site [5,6]. Whilst this kind of corrosion inhibition is often referred to as a barrier effect, i.e., blocking access of the surface to attacking species, in-depth studies have clarified that the most successful inhibitors preferentially adsorb at specific reactive surface sites to stabilise them. This is reported to be effectively a kind of competitive adsorption where the inhibitors have a greater affinity for the surface than the corroding species [7–9]. As illustrated below, NR has been used to characterise such inhibitor layers and has identified significant corrosion inhibition where the organic layer is

present at far less than full surface coverage and significant corrosion where the layer is essentially complete [10].

The complexity of corroding systems necessitates a combination of techniques to fully characterise and understand them. This review focuses on the use of NR; however, it is best used as part of a battery of approaches. Other important complementary techniques include optical microscopy [11], electrochemical methods [12], ellipsometry [13], X-ray and neutron diffraction [14,15], X-ray photoelectron spectroscopy [16] (XPS), secondary ion mass spectrometry [17] (SIMS), atomic force microscopy (AFM) [18], AFM-IR [19] and weight gain/loss measurements [20,21]. There also exist a variety of relatively new elegant synchrotron-based methods [22] such as extended absorption fine structure (EXAFS) [23] and small-angle X-ray and neutron scattering (SAXS and SANS) [24,25]. A summary of some related approaches can be found in [26]. These will not be discussed further in this work.

NR for chemical studies was established in the 1980s with an increase in availability of appropriate facilities and instruments [27]. There has been extensive literature concerning molecules adsorbed at the air/liquid interface, particularly surfactants on the surface of water [26,28–30]. There has also been interest in some particular solid/liquid interfaces over the years, but these have tended to focus on a limited range of substrates such as silicon/silica and alumina, as discussed below. In recent years, an increasing number of substrates have been addressed with this method, including metals and their oxides (particularly iron, nickel, copper, titanium, etc., as detailed below), alloys (such as steel), a range of minerals (such as mica [31] and calcite [32]) and polymers [33]. These new metal-based substrates have permitted more corrosion-oriented investigations.

Importantly, neutron scattering is non-invasive and is not expected to change the structure of the interfaces being studied [34,35]. In addition, neutrons are very penetrating, enabling the use of neutron-transparent windows. Hence, NR can be used to probe challenging systems in situ, including buried interfaces (under liquids) with samples under extreme conditions of temperature and pressure [36–38] and under external fields such as shear [39,40] and/or electrochemical potential [41–45].

In this short review, the NR method and its application to the study of corrosion and its inhibition will be outlined. The advantages and limitations of the technique are described, with a number of important systems presented in greater detail.

2. Basic Introduction to Neutron Reflectometry

The NR technique has been presented in many excellent reviews [26,27]. A brief outline of the method is given below, with particular focus on issues pertinent to corrosion. Figure 1 schematically illustrates the reflection of a collimated neutron beam from an interface. The incident beam is produced by either a reactor source, such as that at the Institut Laue-Langevin in Grenoble, France, or by the spallation process, such as at the ISIS facility at the Rutherford Appleton lab, near Oxford, U.K. This requirement for centralised international facilities may present some access issues for a potential user. Generally, access is obtained by peer review of proposals, typically with calls every six months. Beamline scientists are usually happy to discuss potential applications to help craft the best proposals. These scientists are also extremely helpful in assisting during the experiments themselves. In many cases, they will form part of the collaborative effort of the experiment and will appear on appropriate publications.

The reactors use a fission source (U^{235} or Pu^{239}), while typical spallation targets are tungsten, mercury or uranium. Both methods produce high-energy protons that are moderated to give a more useful range of neutron wavelength [46]. NR often requires access to long wavelength neutrons obtained from a cold source/moderator (e.g., liquid hydrogen) [26].

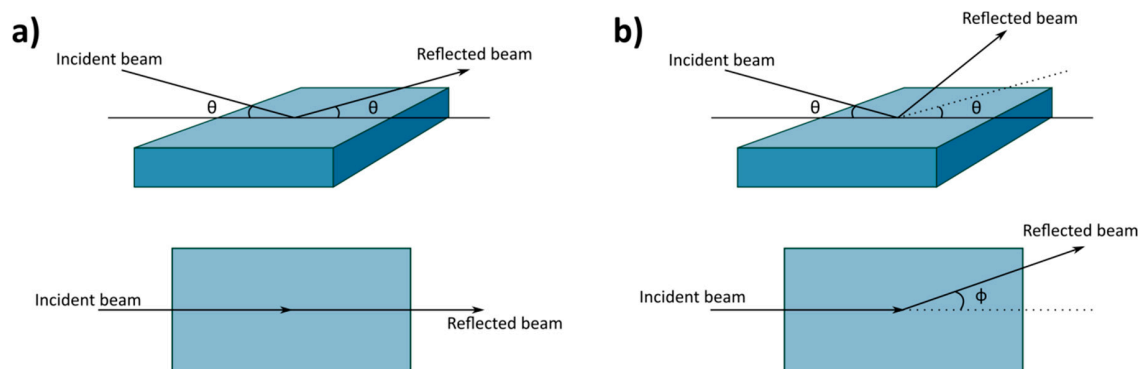


Figure 1. Illustration of the geometry of a neutron reflectometry experiment: (a) specular reflection and (b) off-specular reflection (top: isometric view; bottom: plan view).

The incident beam is directed to the sample position by neutron guides and collimated using slits. The neutrons can then be considered to reflect from the surface. Where the incident and reflected angles are the same, this is referred to as specular reflection, and the majority of studies are performed in this geometry. In this arrangement, the reflected intensity is sensitive to structure normal to the plane of the interface. The detection of neutrons is achieved by reaction with species such as ^3He , ^6Li or ^{10}B , producing charged products that can be detected. The neutron also has a spin $\frac{1}{2}$ arising from its intrinsic magnetic moment, which enables it to interact with unpaired electrons and hence to probe magnetic structures [46].

Dedicated reflectometers at the various neutron sources have particular strengths and weaknesses dictated by their principal applications. More details can be found in reference papers for the instruments (such as CRISP [47], SURF [48], INTER [49], OFFSPEC and POLREF [50] at ISIS, D17 [51] and Figaro [52] at ILL, V6 [53] at the Helmholtz Zentrum in Berlin, AMOR [54] at the Paul Scherrer Institute in Switzerland and many others at institutions outside of Europe).

The work reviewed here is concerned with neutrons that reflect from the interface without the change of energy: ‘elastic scattering’ [55] (quasi and inelastic scattering of neutrons can also be used to probe molecular dynamics, but this is less relevant to present corrosion studies). The specular reflectivity is defined as the ratio of the reflected intensity to the incident radiation intensity. Reflectivity that is not at the same angle as the incident beam may also be used for structural analysis. This is referred to as off-specular scattering and contains information about both the in-plane structure and the structure normal to the interface. However, quantitative analysis of the off-specular scattering is challenging and generally limited to a few specific cases.

As outlined in the Introduction, corrosion can be uniform or localised. When using specular reflection, only changes in the structure perpendicular to the plane of the surface are detected. Therefore, the detailed in-plane structure typical of localised corrosion, such as pitting, is not usually accessed, other than in its contribution to the spatial average across the sample plane.

In specular reflection, the experimental variable of interest is the momentum transfer vector, Q , which is a function of the incident/reflected angle, θ , and the neutron wavelength, λ :

$$Q = \frac{4\pi \sin \theta}{\lambda}, \quad (1)$$

There are, broadly, two types of experiments:

1. Q is varied at fixed incident λ and variable θ .
2. Q is varied at fixed θ and variable λ .

Both approaches can be used at a reactor source. The fixed-angle approach (2) is naturally accommodated at a spallation source where the neutrons are produced in short pulses. The time of flight of the neutrons to the detector provides a convenient method to determine the neutron energy and wavelength. However, it is usual to combine reflection data at several incident angles, as the wavelength range in a single pulse is not sufficient to cover the full range of Q . Specular reflection requires only a single detector; however, it is not uncommon for a multidetector to be used as this provides a convenient method to identify and remove background scattering and can also be used to access off-specular scattering.

Figure 2 illustrates a simulation of a typical reflection dataset for a thin film on a solid substrate, with reflectivity on the y -axis and the momentum transfer, Q , on the x -axis. The characteristic critical edge is seen at low Q ; at small incidence angles, total reflection occurs until a critical angle, θ_c , is reached, the value of which is a sensitive measure of the composition of the two bulk phases. In many cases, the reflection data can be collected in absolute units; however, the intensity below the critical angle should be unity, providing a convenient intensity scaling. There are cases where this is not appropriate, for example where there is significant beam attenuation [31,56,57].

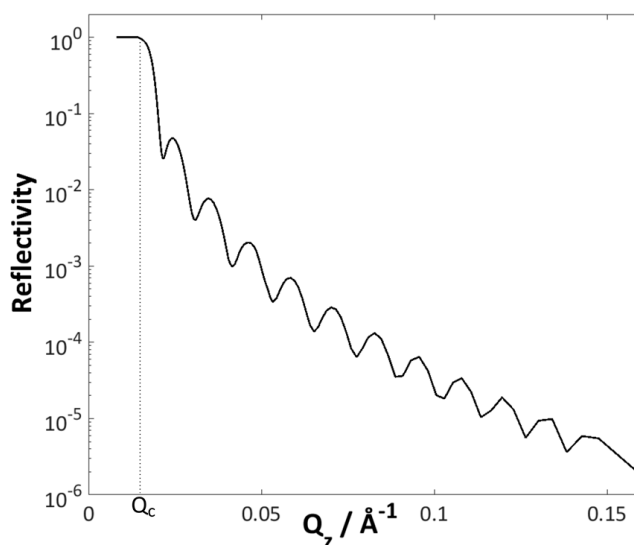


Figure 2. Representative simulation of neutron reflectometry data, illustrating the total reflection at low Q and the fringes that arise from an adsorbed layer at higher Q . The critical edge is marked as Q_c .

The simulation also illustrates the characteristic fringes that arise from the presence of a deposited layer at the surface. These fringes arise from interference from reflection at the two interfaces that bound the thin film. The period of the fringes is therefore related to the film thickness and their amplitude to the composition of the thin film. In some cases where the films are very thick, the calculation of the reflected signal is more complex [31,56,57]. However, for the corrosion-related work discussed here, the thin film approximation is almost universally used.

The experiment generally requires the substrates to be very flat (ideally $<5 \text{ \AA}$ roughness). Any roughness affects the scattering at high Q to a certain extent, but in extreme cases the surface becomes so rough that the total reflection region also falls in intensity. This arises when the surface scatters neutrons in all directions, rather than as a well-directed specular beam, and hence, not all of the specular beam reaches the detector. However, this is a very convenient method to identify corrosion-induced roughening of a substrate, although quantification of this roughening can be complex. It is important to be aware that the preparation of substrates appropriate for NR experiments may result in ideal surfaces that are not necessarily an accurate representation of realistic samples; the combination of NR

with other surface characterisation techniques, such as XPS or TOF-SIMS (time-of-flight secondary ion mass spectrometry), is therefore advisable.

The NR technique has very high spatial resolution allowing the study of sharp metal interfaces in the angstrom range. However, the fluxes of even the world's most intense neutron sources are relatively low, and hence to make best use of the resource, the high resolution that would be available with a very narrow finely-focused neutron beam is often compromised to give shorter count times by opening up the beam to gain more flux at the expense of the resolution (typically 4–6% $\Delta Q/Q$).

The object of the reflectometry experiment is to deduce the real space structure, expressed as the variation in scattering length density with positional coordinate, z , in real space, from the measured reflectivity profiles in Q space [46]. Similarly to diffraction, there is generally no unique inversion method from scattering to real space. The approach generally used is to compare experimental data to that calculated based on a structural model fit. There are several programmes available for this (e.g., MOTOFIT [58], RASCAL, GenX [59], amongst others), often using the optical matrix method [26,27]. The use of contrast variation, discussed below, is often used to constrain the fitting process. Although seldom exploited in practice, polarised neutron analysis and related approaches can be used to determine phases in favourable cases, for example using magnetic reference layers [60].

3. SLD/Contrast Variation and Matching

One of the great strengths of neutron scattering lies in the use of contrast variation arising from the apparent independence of neutron scattering on position within the periodic table, in contrast to X-ray scattering, which is dependent on electron density. This is a particular strength when considering corrosion inhibition as neutrons are able to characterise organics just as easily as metals, rather than being more sensitive to heavier elements. A list of selected scattering lengths is presented in Table 1. It is particularly noteworthy that the difference in scattering length between two isotopes of the same element is often significant; for example, particularly between H and D. This is a key asset for neutron work, as explained below. An example of the difference in reflectivity profiles for two different isotopes, ^{58}Ni and ^{62}Ni is shown in Figure 3. Formally, the scattering length can be complex, where the imaginary part reflects absorption of the neutrons. For most of the systems considered here, this is usually considered to be zero. However, there are cases where thick films do require an attenuation correction [31,61,62].

The scattering length can also have a contribution arising from magnetic interactions of the neutrons with the sample, due to the magnetic component of the neutron refractive index:

$$n_{\pm} = n_{\text{nucl.}} \pm n_{\text{mag.}} = \frac{1 - N\lambda^2(b \pm C\mu)}{2\pi}, \quad (2)$$

where n is the refractive index, N is the atom number density, λ is the neutron wavelength, b is the neutron scattering length, μ is the average magnetic moment and C is a constant. Hence, for any material with a magnetic moment ($\mu \neq 0$), two possible values of scattering power exist. This facet is exploited in polarised neutron reflectometry (PNR) in two main ways: firstly, and most commonly, analysis of the change in polarisation of the neutrons after interaction with the sample can be related back to the sample's magnetic qualities [63,64]. Alternatively, and more powerfully for the corrosion studies of interest here, the incident beam can be polarised firstly up- and then down-spin and two reflectivity profiles collected for the same system, with the scattering power of the magnetic metal layer differing for each [64]. As the analysis of neutron reflectometry data involves fitting a simulated model to the experimental data, this permits a greater confidence in the fitted model by constraining the fits. Furthermore, it permits the experimenter to 'tune' the metal contrast to the most helpful value relative to other elements in their system, so that specific parts can be emphasised.

Table 1. Some scattering lengths for elements of particular interest in this context (those without the isotope specified are weighted by the natural abundance due to the lack of significant variation).

Atom	Scattering Length, $b_i/10^{-15}$ m	Atom	Scattering Length, $b_i/10^{-15}$ m
H	−3.74	D	+6.67
C	+6.65	^6Li	+2.00
O	+5.80	^7Li	−2.22
N	+9.36	Al	+3.45
Si	+4.15	^{58}Ni	+14.40
^{54}Fe	+4.20	^{60}Ni	+2.80
^{56}Fe	+9.94	^{61}Ni	+7.60
^{57}Fe	+2.30	^{62}Ni	−8.70
^{58}Fe	+15.70	^{64}Ni	−0.37

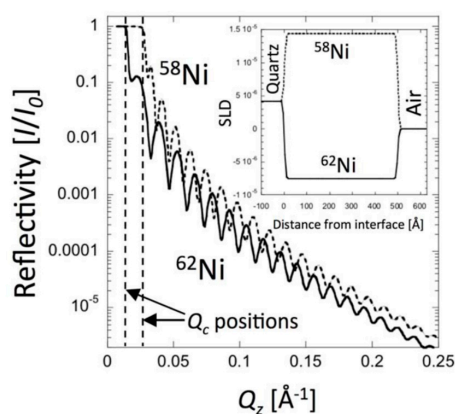


Figure 3. Simulated reflectivity curves for 500 Å films of ^{58}Ni (dashed line) and ^{62}Ni (solid line) on a quartz substrate, with scattering length density (SLD) profiles shown in the inset. Reproduced with kind permission from [46], MDPI, 2016.

Figure 4 shows some representative PNR data for an iron film on a silicon substrate collected on the POLREF instrument at ISIS; as is evident, the up-spin data are completely different from the down-spin [65]. By requiring a single structural model that fits both datasets, the possible structural solutions are constrained. A disadvantage of using PNR is that half the neutron beam is lost for each polarisation [26], requiring longer count times to get good data; this may be a drawback for kinetic studies in particular.

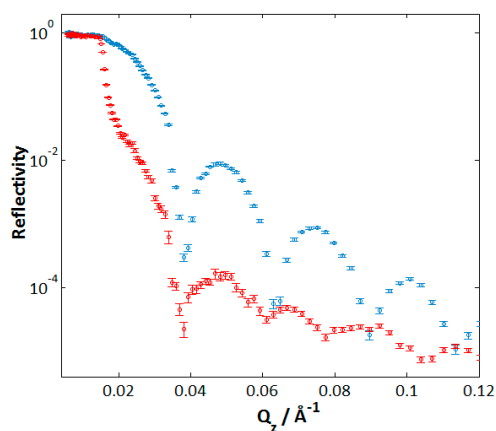


Figure 4. Example of polarised neutron reflectometry (PNR) data collected for a Fe film on silicon substrate, showing up-spin (blue) and down-spin (red) data collected on POLREF at the ISIS neutron source (doi:10.5286/ISIS.E.24088548).

In calculating the reflectivity, the interface is considered to comprise a number of layers with different compositions. Each layer will comprise different elements/isotopes. The extent by which each material scatters neutrons is given by the scattering length density (SLD), defined in the equation:

$$\text{SLD} = \frac{\sum_i N_i b_i}{V}, \quad (3)$$

where b_i is the scattering length of the isotope in question and N_i is the number of the atoms of isotope i in a volume V .

A selection of SLDs for some relevant materials is given in Table 2. As inferred from the disparity of scattering lengths for H and D earlier, the SLDs of H₂O and D₂O are also very different, despite being essentially identical chemically. Therefore, by mixing heavy and light water at the correct ratio, a solvent of any SLD can be obtained between the two extremes of pure H₂O and pure D₂O. This is called contrast variation and is an extremely powerful facet of the NR technique.

Table 2. Scattering length densities (SLDs) of some representative molecules/materials’.

Species	SLD/10 ⁻⁶ Å ⁻²
H ₂ O	−0.56
D ₂ O	+6.34
H-Dodecane	−0.46
Dodecane-d ₂₆	+6.71
Si	+2.07
SiO ₂	+3.63
Fe (up-spin)	+12.99
Fe (down-spin)	+3.05
Fe (non-polarised)	+8.02
Fe ₂ O ₃	+7.18
Ni (up-spin)	+10.86
Ni (down-spin)	+7.94
Ni (non-polarised)	+9.41
NiO	8.66
Ti	−1.91
TiO ₂	2.63

The reflected signal arises when there are differences in SLD between regions of the sample. If two regions have the same SLD, there is no contrast and hence no signal. Therefore, by contrast-matching, components of a given system can be made to disappear; this is particularly useful for complex multicomponent systems, for which scattering from all but a single component can be ‘switched off’ in order to more simply emphasise that one layer or component. By then changing contrasts and repeating, another component may be highlighted. In this way, the system may be characterised in full. This is clearly extremely powerful for corrosion studies, as the corroding metal, oxide layers and any organic species such as an adsorbed corrosion inhibitor may be selectively studied simultaneously and in situ. Whilst the costs of deuterating species are often high, many neutron facilities have well-established deuteration facilities.

4. Experimental Setup

For the corrosion studies of interest in this review, the solid/liquid interface is of most interest. A typical solid/liquid cell is depicted in Figure 5, in which the liquid is held in a trough clamped against the solid surface. The smallest volume of solution possible is usually accommodated due to the expense of deuterated organic solvents. However, the trough should not be made too shallow in case reflection from the lower surface interferes with that from the interface of interest. The trough surface is sometimes roughened to prevent significant scattering from reaching the detector. Another approach has been to put a thin liquid drop between two substrates, held in by capillary forces [26,66].

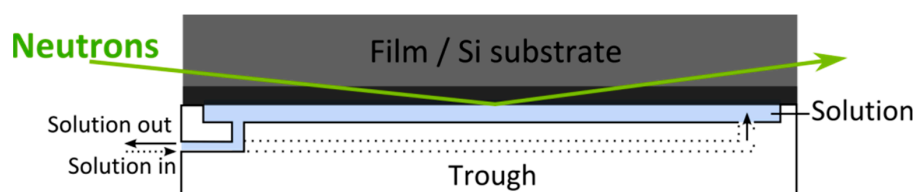


Figure 5. Schematic of a typical solid/liquid cell.

For solid/liquid cells, the interface in question can be mounted either horizontally or vertically. This contrasts with studies of the air/liquid surface where the plane of the liquid surface must be horizontal [66]. Other potential issues such as trapped air bubbles must be considered; these may be avoided by careful filling of the cell in an upright position. Furthermore, changing solvent contrasts may require several flushes through the cell to ensure complete exchange.

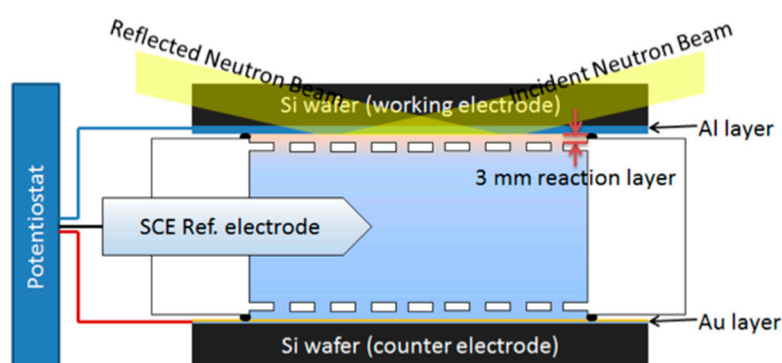


Figure 6. Schematic of the NR electrochemical cell used by Dong et al. where reflectivity measurements are taken from the working electrode (Al film on Si) to monitor its corrosion at different applied potentials. Reproduced with kind permission from [67], ACS Publications, 2011.

Specialised neutron cells have also been custom-made for specific applications, such as extreme temperatures, pressures or for investigating systems under shear [39,40]. Most relevant to the topic of corrosion are cells designed to accommodate simultaneous electrochemical measurements by incorporation of various electrodes into the cell so that structural data can be collected over a range of potentials, for example [41–45]. Care must be taken to prevent the electrodes from contacting with the surface of interest, given the small volume of trough usually used, although larger cells that accommodate ‘bulky’ electrodes such as saturated calomel electrodes have also been used successfully [68]. The schematic of a cell used in a combined electrochemical and neutron reflectometry experiment is shown in Figure 6.

5. Substrates

Substrates (metal/metal oxide surfaces) are generally as large as possible to maximise use of the neutron beam, which has much lower flux than related techniques such as X-ray reflection. As the neutron beam comes in through the substrate and is reflected back through it, the substrate must be sufficiently transparent to neutrons to prevent significant attenuation. This requirement has led to silicon/silica and alumina being more extensively studied than other materials as they have excellent neutron transmission [69–72]. They can also be obtained as single crystals of relatively large dimensions that can be polished very flat ($\sim <5 \text{ \AA}$).

Although other substrates of interest often exhibit transmission that is too low for these experiments, an effective approach to study highly-absorbing materials has been to deposit thin films onto a transmitting substrate (such as silicon). This has been successfully applied to a range of

materials, such as iron [65,73,74], copper [10], titanium [41], nickel [75], chromium [76], zirconium [77], ITO [78], stainless steel [76] and various other alloys [79–82]. Care should be taken during deposition and subsequent handling to ensure that the final surface represents the material desired: for example to what extent it oxidises upon exposure to air. Our neutron reflectometry experiments are usually combined with XPS to characterise the exact surface species present. Depth profiling with XPS or SIMS are also helpful in uncovering any inhomogeneity in the deposited layers, particularly for alloys. The deposited layer should be thin enough to prevent significant neutron absorption; thicknesses of the order 10–1000 nm are usually chosen in order to give well-resolved fringe structures and hence easily detect adsorbed layers.

The cleaning process for the substrate prior to the NR experiment is a crucial consideration, as any surface exposed to ambient conditions will be covered in organic matter within a few seconds, which will be observed in the NR data. Cleaning procedures will depend on the particular material being used. Ideally, freshly deposited films should be kept clean by careful handling. Whilst acid-treatments will be appropriate for inert materials, such as silicon, they will quickly dissolve iron films, which are best cleaned using UV/ozone, although this will lead to more extensive oxide formation. All parts of the cell are generally cleaned with strong acids/related detergents to minimise any contamination.

6. Examples of Metal Corrosion Studies Using NR

A significant body of neutron reflectometry papers concerning the corrosion and corrosion prevention of a range of metal surfaces in different conditions has been published. A brief review of these is given below.

6.1. Aluminium

Aluminium is a particularly promising material for neutron reflectometry studies as there are two main methods by which appropriate samples may be relatively simply prepared; firstly, the common method of depositing a thin film of the metal onto a silicon or quartz substrate; however, for studies more interested in the passive Al_2O_3 layer, a single crystal of polished sapphire is often used, as it has a high transparency to neutrons. Unsurprisingly, therefore, aluminium has been fairly well studied using this technique, with a body of work looking at phenomena such as adsorption of organic molecules and the behaviour of the adsorbed materials under shear condition [39,69–72,83–86]. A small handful of studies relevant to corrosion also exist, as outlined below.

As an example of using a custom-made NR cell to monitor the effects of extreme environments on corrosive behaviour, Junghans et al. used NR to monitor the surface aluminium oxide layer as hydrostatic pressure was increased. They observed a decrease in the oxide SLD at pressures of 600 atm, thought to arise from incorporation of Cl^- ions into the layer [87]. As the oxide and metal thicknesses stayed constant throughout, NR provided a unique opportunity of observing this subtle chemical change in situ.

Wang et al. characterised in detail a vanadate-based protective film spin-coated on aluminium. They noted the necessity of using two structural layers to characterise this film, with a smaller, denser vanadate coating at the aluminium surface and a thicker, more porous upper layer. Exposure to D_2O vapour and subsequent monitoring of the changes in SLD demonstrated that the upper layer is permeable to water, whereas the SLD of the dense innermost layer remained constant. They concluded that the corrosion inhibition results entirely from this impermeable innermost layer at the surface [88].

Hu et al. combined small-angle X-ray and neutron scattering (SAXS and SANS) with X-ray reflectivity (XRR) and NR to build up a better model for the structural changes of anodised aluminium, which is used to provide a more corrosion-resistant surface layer. The anodised aluminium (AA) layer was found to comprise two layers: a thin non-porous barrier oxide covered by a very thick porous layer comprised of a hexagonal array of pores. This must be sealed (usually with nickel acetate at elevated temperatures) to ensure good protection. Interestingly, the authors found that the modification of conditions for the reflectivity measurements (e.g., limited currents) led to a different structure to

that observed with the other techniques where the current was unlimited. Whereas the SAXS and SANS results showed varying penetration of the different sealing agents, the AA films studied by NR appeared to have their pores capped during the anodisation process [89]. Their work demonstrated the high desirability of combining a range of complementary techniques to study a corrosion system.

Dong et al. reported the passivating nature of a trivalent chromium process (TCP) film on aluminium exposed to corrosive salt solutions under anodic potentials. A thin layer of D₂O was found to penetrate between the TCP film and underlying metal, but the film retained its corrosion inhibition, which was attributed to its ion barrier properties. When the potential was increased beyond the pitting potential, passivity was lost, and the aluminium metal dissolved. The TCP film was found to significantly swell at these potentials and hence allow penetration of the salt ions that attack the underlying metal [67].

6.2. Titanium

The titanium/titania surface and its behaviour in corrosive conditions are fairly well-represented in the literature. It is, naturally, the passive TiO₂ layer that is of most interest, particularly since depositing a pure (oxygen-free) layer of the titanium metal itself has proven challenging [77,90]. Uneven oxide permeation into the metal layer over time was further observed by Miller after remeasuring a titanium film four months after its preparation and seeing a loss in NR fringe definition, emphasising the importance of using freshly-prepared samples for neutron studies [17].

Changes in the passive titania layer in aqueous solutions over a range of applied potentials have been observed using NR. Importantly, hydrogen ingress into the oxide film can be seen by a lowering in SLD under applied cathodic potential [17,41,68,91]. Tun et al. modelled this oxide as comprising two distinct layers, with the lower-SLD region getting thicker and the higher-SLD layer dissolving as a cathodic potential is applied, whilst the overall oxide layer thickness remained constant. They postulated that the hydrogen content is probably mostly in the form of OH⁻ [41]. Wiesler et al. observed the roughness and corrosion of the oxide film under an applied cathodic potential to such an extent for it to lose its passivity and for the underlying metal film to start dissolving, shown by the fitted SLD profiles in Figure 7 [91].

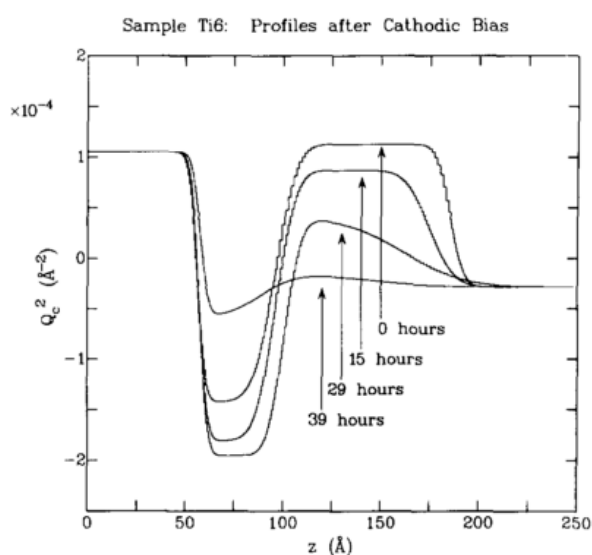


Figure 7. SLD profiles for a Ti film on Si under cathodic polarisation (−2 V) over time; the ingress of H is shown by the drop in SLD of the oxide layer and the increase in SLD of the metal (which has a more negative SLD than H). Reproduced with kind permission from [91], Elsevier, 1994.

Wiesler et al. further studied titanium/titania under a more corrosive sulfuric acid (0.1 M) environment and observed dissolution of the oxide layer in situ at a rate of 0.7 \AA h^{-1} . Interestingly, they observed that titanium was self-healing when anodic potentials were applied, in that the metal below the oxide re-passivated itself, but that no self-healing mechanism occurred under a cathodic bias [92]. This work highlighted the ability of NR to determine detailed structural information concerning buried layers that are almost impossible to distinguish using other techniques; for example, the titanium metal and titanium oxide layers appear essentially identical to X-rays, yet scatter neutrons significantly differently.

6.3. Zirconium

Zirconium is often used in the nuclear industry due to its high corrosion resistance, although this can be reduced if exposure to water leads to H ingress. Zirconium has been studied in comparison to titanium by Noël et al. as it exhibits some similar characteristics in that its surface is usually covered by an oxide layer and that it also readily absorbs hydrogen to the detriment of its mechanical stability. However, in contrast to titanium, both zirconium and a zirconium-lead alloy were seen to suddenly form cracks at a potential of around 1.5 V. Electrolyte solution immediately occupied these cracks, recorded as a drop in SLD. When the anodic bias was removed, the oxide healed itself, and the cracks were refilled with new oxide. In further contrast to titanium, no hydrogen ingress was observed for cathodic bias [77,79]. Their work demonstrated the power and potential of coupling EIS measurements with in situ NR.

The ingress of H as a function of pH was further studied by Noël et al., whereby the potential was kept fixed at -1.6 V and the pH lowered by the addition of H_2SO_4 . The NR results showed that the zirconium and passive ZrO_2 layer retained their thicknesses at all pHs, but that their SLDs were seen to decrease at acidic pH, pointing to an ingress of H. Interestingly, when the pH was kept at 2.0, but the -1.6 V potential switched off, the SLDs were seen to return to close to their original values, suggesting a high environment-dependent H mobility in and out of the films [93].

6.4. Nickel

Nickel's magnetic behaviour means it can be studied by polarised neutrons; as discussed above, the SLD of any magnetic material differs when exposed to up- or down-spin neutrons, and so, two 'contrasts' may be obtained without changing any of the sample, an approach that is particularly useful for buried nickel layers, for example [94].

Singh et al. recorded NR profiles for a pristine nickel layer pre- and post-exposure to a pH 3 chloride solution. After exposure to the corrosive environment, a one-layer model was no longer able to describe the system, and a seven-layer model was used, with areas of lowest density at both the nickel/air interface, as might be expected, but also surprisingly at the silicon/nickel interface. The authors attributed this to pit formation and a network of voids growing under the nickel surface [95]. They further used off-specular NR and PNR to simultaneously measure the chemical and magnetic roughnesses of a nickel film deposited on glass and exposed to atmospheric conditions for 15 years. The aged film was split into two layers: a 1200 \AA layer of normal density nickel topped with a 235 \AA layer of reduced density, which they attributed to the growth of a void network due to atmospheric corrosion [95,96]. The authors extended this approach by subjecting a nickel film to chloride solutions and using off-specular and specular NR to monitor the corrosion. As for their earlier study, the decomposition was found to be non-monotonic with depth, suggesting that once the air/film surface had been penetrated, there was extensive in-plane corrosion below the surface. The off-specular scattering was used to infer the height-height correlation function of both buried and exposed interfaces. The as-prepared surface had a correlation length of approximately 800 \AA , whilst that of the corroded surface was approximately 1200 \AA , which was reported to be typical of the pit width. By combining the NR data with AFM studies, they demonstrated the power of this approach to fully characterise the corroding system in situ at the angstrom-level [97].

Wood et al. used PNR to examine the effects of different potential corrosion inhibitors on the corrosion of nickel in an acidic environment. By using two water contrasts—H₂O and D₂O—they were able to effectively contrast-match to the surfactant layer and nickel surface respectively and hence collect data pertaining to each specific part of the system in situ, as demonstrated in Figure 8. Importantly, they were able to demonstrate excellent corrosion inhibition at very low pH using sodium dodecyl sulphate (SDS) at a surfactant coverage of only 60%, corroborating the view that full coverage of inhibitor is unnecessary for protection of the surface [75]. This critical finding is believed to arise from the presence of ‘active sites’ at the metal surface that are particularly prone to corrosion and hence nucleate dissolution of the metal. By binding specifically to these active sites, the surface is effectively passivated [98,99].

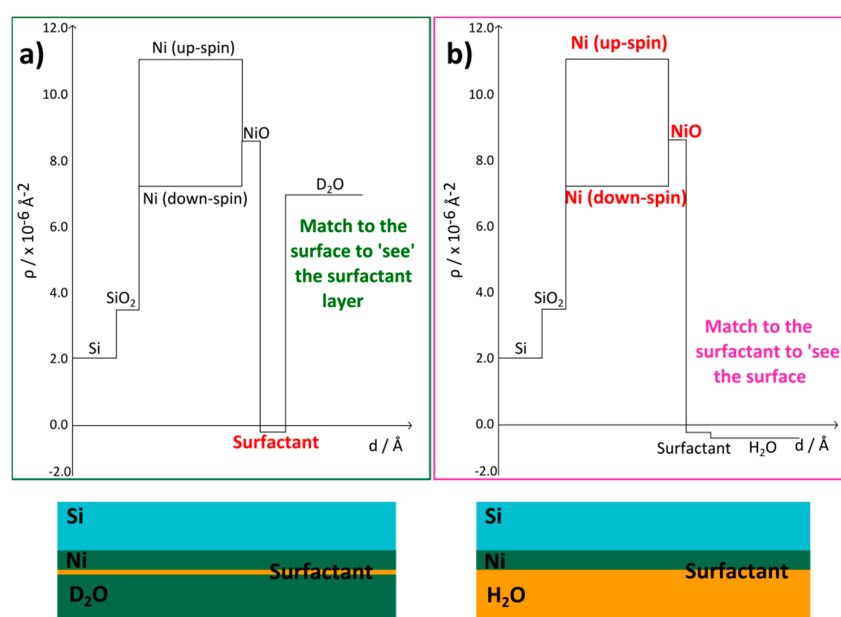


Figure 8. Simulated SLD profiles for the nickel/surfactant/acid system in (a) D₂O and (b) H₂O, showing how use of the different contrasts allows emphasis on different components of the system. Reproduced with permission from [75], ACS Publications, 2015.

Another example of combining NR and electrochemical measurements is found in the work of Saville et al. They collected data on a short timescale to monitor ion and solvent trapping within a nickel hydroxide film as the potential was cycled and saw a hysteresis of reflectivity as the film was oxidised and reduced. They attributed this to the release and capture of positively-charged D⁺ and Li⁺ ions; these were very subtle changes that would have been hard to detect using other methods [100].

6.5. Iron and Steel

Despite the importance of iron and steel across a wide range of industrial applications, they remain relatively unstudied as a surface by neutron reflectometry, although a small but significant body of work concerning surfactant adsorption at iron/liquid interfaces does exist [65,73,75,101–103]. The direct study of steel alloys is slightly more challenging due to the necessity of preparing thin (to ensure neutron transmission) and very flat films, although recent work has demonstrated that representative stainless steel films can be prepared using electron-beam deposition at low pressures [76].

As for nickel, the use of polarised NR is particularly powerful for iron studies. The difference in the SLDs for iron under the two polarisation states is very large, due to its high magnetic moment, being $3.06 \times 10^{-6} \text{ \AA}^{-2}$ and $12.99 \times 10^{-6} \text{ \AA}^{-2}$ for down- and up-spin neutrons, respectively. This provides great scope for the selection of contrasts to best emphasise components of interest. Kruger et al. further highlighted the power of PNR by demonstrating its ability to distinguish between

non-ferromagnetic oxides and hydroxides (such as Fe_2O_3 and FeOOH) and ferromagnetic ones (Fe_3O_4) using an electrochemical cell to grow the oxide layers [104]. Feng et al. used a similar approach twenty years later combined with X-ray reflectivity and found the oxide layer on their samples to be non-ferromagnetic [105].

Wood et al. recently combined XRR and NR for an in-depth study of iron corrosion in a range of subtly different environments; whilst the X-rays were particularly powerful in monitoring the growth, dissolution and roughening of oxide and metal layers, NR was invaluable in characterising the adsorption of organic inhibitors and simultaneous protection or dissolution of the metal in situ. Interestingly, the combination of techniques raised a crucial distinction: it was discovered that the treatment of the samples in preparation for NR in fact afforded them unexpectedly significant corrosion protection, an observation later verified by XRR [106].

6.6. Copper

The chemistry of copper depends in large part on the exact composition of the surface layer; copper metal and the various oxides (CuO and Cu_2O) can be distinguished by XPS (via the shake-up structure or Auger LMM peaks) and in small, but significant differences in their neutron SLD values, as exemplified by Welbourn et al., who combined these two techniques to consider the corrosion of copper films in oil. They examined the effects of two potential corrosion inhibitors—a fatty amine and a thiol—on the corrosion of copper in an oil environment exposed to elemental sulphur. Their analysis allowed a detailed breakdown of the copper layer into oxides and hydroxides, which showed different behaviour under corrosive conditions. Similarly to the work by Wood et al. [75], the NR technique was shown to be a powerful tool to characterise both the adsorbed inhibitor and metal surface by the use of contrast-matching. Their work also supported the view of corrosion inhibition as a mechanism that blocks specific active sites: whilst the amine layer coverage was only around 65%, compared to around 85% for the thiol layer, it proved to be a far better inhibitor. The authors used XPS to link this behaviour to the reductive effects of the thiol on the Cu(II) oxide at the surface, rendering it more prone to corrosion [10].

6.7. Tantalum

Rieker et al. demonstrated the power of NR to distinguish between differences in passive layers formed in different conditions by subjecting thin films of Ta_2N on silicon to annealing under vacuum, hydrogen and air. Whilst only Ta_2N was seen to form in vacuo, a 90 Å layer of TaH_x was formed at the surface when hydrogen gas was used. When the annealing occurred in open air, the resultant layer was visibly cracked and found to consist of barely any Ta_2N , but a thick layer of TaO_x [80].

7. Corrosion Related NR Work

7.1. Electrochemical

Corrosion is often studied as an electrochemical process, as already demonstrated above by the use of electrochemical NR cells to investigate controlled metal dissolution. There have been a number of related NR studies with in situ electrochemistry addressing an interesting range of challenges such as battery electrodes [107–111], solid electrolyte interface SEI formation [84], electroactive polymer films [112–114] and other double layer capacitance systems, such as ionic liquids at surfaces [56,115,116], as well as the formation and properties of passivating oxide layers [68,91,100].

There are some interesting reviews of certain aspects of this area [26,117] that provide an outline of the key role of NR as an in situ probe for electrochemical systems. Recent important examples are those related to energy, such as supercapacitors, batteries and fuel cells, where the key physics occurs at an interface. Other experimental methods used to probe these important systems can be rather limited, particularly when conducted ex situ, and often lead to a loss of information and/or artefacts [117].

NR contrast variation is extremely helpful for electrochemical studies, particularly for systems containing light elements; for example, lithium ion battery anode and cathode materials [84,117], which cannot be easily detected by XRR. NR offers other advantages over other approaches used to study electrochemistry, which are often limited in their ability to study interfacial structures in situ due to the large volume of liquid relative to the fraction of molecules at the surface, leading to any signal arising from interfacial structure being swamped by that from the bulk. The liquid may also attenuate signals from optical methods and prevent the use of UHV surface study techniques. Other methods such as NMR lack depth resolution. The challenges with NR rather centre on the relatively poor flux, which can limit kinetic measurements, and the need for access to international facilities. An overview of the relative merits and limitations for NR and other techniques with respect to electrochemical studies is presented in [117].

The long measurement timescale for NR measurements (1–2 h) can be greatly improved by a number of approaches. These include measuring over a limited Q-range that can be collected quickly (a range with the greatest expected change is chosen) [101] or, perhaps more elegantly, by taking stroboscopic measurements [112,114], in which the potential is cycled and the reflected counts are binned into small time slices. Only a few counts are collected per cycle, but by repeating the process many times, the narrow time slices can yield good statistical data. For example, Glidle et al. used this stroboscopic method to characterise the electrochemical behaviour and permselectivity of electroactive polyvinyl ferrocene (PVF). They found that the modelled polymer film was resolved into three separate layers, with the uppermost showing most solvent intrusion and that closest to the electrode having a lower SLD than the rest of the film (shown by the fitted SLD profile in Figure 9). By using NR in the time-resolved fashion described above, they were able to study the variation of solvent and salt movement through the film as the potential was cycled, finding that the movement of both was less at a higher potential scan rate. They were able to successfully establish the point at which permselectivity failure occurred [114]. One important limitation of stroboscopic measurements is that the process must be completely reversible, and so it may be less useful for corrosion studies if irreversible effects, such as dissolution, are of interest.

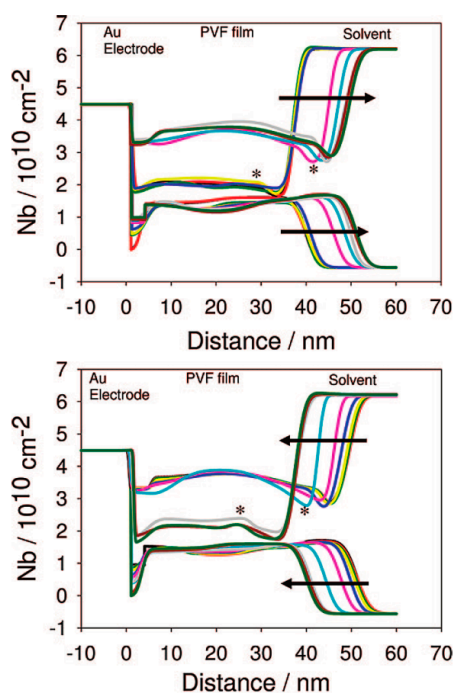


Figure 9. Fitted SLD profiles showing the exodus and ingress of solvent into the uppermost section of a PVF layer deposited on an Au film as potential is cycled from 0.15 V–0.60 V (top) and back again (bottom). Reproduced with kind permission from [114], ACS Publications, 2008.

7.2. Electroactive Polymer Films

Further to the work by Glidle et al. discussed above, there is a series of papers addressing electroactive film structure, particularly looking at polyvinyl ferrocene (PVF) and polyvinyl pyridine (PVP)-based films with coordinated metal ions and various backbone modifications. The focus is on the internal film structure, which is often found to comprise three layers, and how that changes/swells upon electrochemical conditioning. These materials are used for electrochromic applications, as well as energy storage and have interesting conductivity and catalytic properties. NR is used to monitor swelling of the films on exposure to solvents with different anions and the location of key species in the films. The rates of transport of species through the film under different electrochemical conditions are of particular interest [112–114,118–120].

7.3. Silane Barrier Films

Silane barrier films are studied as models for a variety of applications including adhesion promotion, durability and corrosion resistance [55,121–127]. There is a good summary of the field in [123]. These silane films are of increasing interest as replacements for other corrosion inhibitors such as chromates [55]. The overall concept is that the silane monomers hydrolyse and make a highly crosslinked thin film that acts as a barrier. The more hydrophobic the films and the more highly crosslinked, the lower the water migration. The crosslink density and water migration can both be determined by NR. Although the evidence suggests that water is still able to migrate through these films reasonably quickly [121,125], transport of other species is inhibited, which can have a significant corrosion inhibition effect [126].

The films are reported to have a complex multilayer structure, with the regions closest to the substrate and to the air having different structures to the bulk of the film; for example, a greater extent of crosslinking is found at the interfaces [55,128], which can be identified as these regions do not swell in the solvent. The films generally include significant void space, which can be as much as 30% [121]. NR has been used to track the migration of small molecules through these complex films; for example, the extent of salt exclusion, which is a key factor in corrosion inhibition, in particular the prevention of pit formation [126].

The films have been found to swell upon exposure to solvent vapours (such as nitrobenzene); the solvent has often been observed to remain in the silane film layer even after drying [55]. Extended exposure to water leads to breakdown of the silane films, which can also be monitored by NR. For example, Yim et al. combined X-ray reflectivity (XRR) and ATR-IR with NR to study the conditioning of silane films at 80 °C and saw a significant change in structure in the outermost layer of the film, which has no siloxane bonds and so readily dissolves upon exposure to water. The middle layer, in contrast, is chemisorbed to the underlying substrate, and the layer closest to the interface is a monolayer with a high density of bonds to the substrate (shown schematically in Figure 10). Of particular interest is their observation that whilst the layer hydrolyses rapidly upon exposure to H₂O, it does so very slowly when exposed to D₂O, which they attribute to the difference in polarisability of the O-H and O-D bonds [122]. It is useful to bear in mind that whilst isotopic variation is extremely useful in NR to gain different contrasts, it cannot always be taken for granted that the chemistry will remain unchanged, although examples of differences are rather rare.

Whilst it has been reported that the roughness of the silane film is an important factor in its corrosion inhibition, off-specular scattering has indicated little or no in-plane structure [128]. However, NR experiments have been performed on films that are significantly thinner than those used commercially. For truly effective corrosion inhibition and protection against crack formation, the films are required to have at least 2000 Å thickness [123]. The water uptake of some films (for example, bis sulfur silane films) has been found to depend on their thickness, with the thicker films showing higher porosity and hence water uptake. The water uptake is also related to the temperature of film formation; at higher temperatures, the films are denser and hence have better water barrier properties [123].

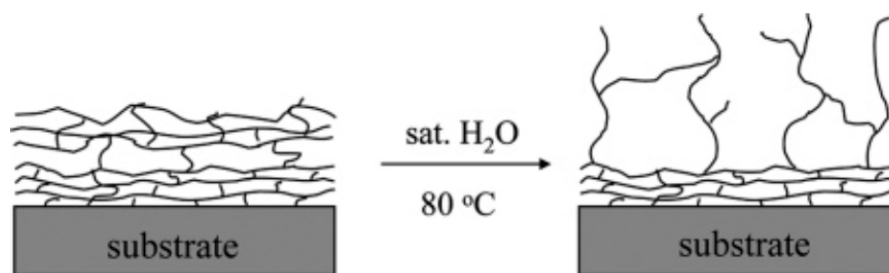


Figure 10. Schematic of silane film structure pre- and post-exposure to water, as determined by the NR model fit. Figure reproduced with kind permission from [122], ACS Publications, 2005.

In a related area, Lechenault et al. used NR to monitor the effects of stress corrosion on silicate glasses. As they were interested in the effects of the corrosion on specific localised defects on the glass, they used neutron-absorbing materials to block the beam at all but the areas of interest and counted over very long times (48 h) to get good data. The water was found to penetrate to greater depth at cracked areas on the silicate glass surface, which they attribute to a chemical degradation of the glass network [129].

7.4. Other Corrosion-Inhibiting Coating Studies

As already detailed, NR is an excellent tool for studying thin organic layers along with their level of efficacy in protecting underlying metal surfaces. Unsurprisingly, therefore, it has been used to characterise the corrosion protection of a variety of different coatings, including bio-inspired adhesive polymers in which catechol groups bind to the metal surface to provide a highly effective water barrier [124].

Superhydrophobic coatings have also been extensively investigated for their corrosion inhibition potential. Barkhudarov et al. used NR to investigate superhydrophobic aerogels deposited onto aluminium and saw a ten-fold decrease in the corrosion rate for the protected surface compared to the bare metal. The increasing thickness and SLD of the Al_2O_3 layer and simultaneous dissolution of the Al metal were used to monitor the corrosion, although they were unable to directly observe water ingress under the aerogel layer due to the resolution restrictions of the instrument [130].

7.5. Battery Material Studies

Understanding the behaviour of materials such as lithium and other battery materials is of great academic and industrial interest. As outlined above, NR is particularly powerful in studying light materials such as lithium, even more so when different isotopes are used to change the contrast [111]. There are several papers coupling electrochemistry and NR to study model battery materials, many of which address the movement of lithium into other materials, such as silicon, under different conditions [107–110]. Lithiated silicon is a key material for batteries and exhibits a ‘solid electrolyte interface’ (or interphase) in the cell. This can form a barrier against redox activity, and so understanding its composition, thickness and porosity has been a key question for NR to address. Recent work studied the development of the SEI as a function of potential and found it to be 4.5 nm thick after 10–20 cycles, growing to 8.9 nm after a simulated charge/discharge cycle [84].

7.6. Ionic Liquids

The structure of ions adjacent to an electrode for use in supercapacitors has been studied by using NR to look at electrode/ionic liquid interfaces. This electric double layer structure is of key importance both for electrochemical and corrosion applications. Lauw et al. used NR to characterise the ion surface excess of an ionic liquid at the surface of a gold electrode as potential is varied. Interestingly, they found there remained a cation surface excess even when the surface was positively charged, although

at a lower concentration than when negatively charged. They ascribed this to the specific adsorption of the cation overcoming the electrostatic effects [115,116].

8. Conclusions

Neutron reflectometry has been used to study a range of corroding systems and related phenomena, although it is far from being used to its full potential in this area. As we have outlined, it is an extremely powerful, non-destructive tool to monitor several characteristics of the in situ corroding system at the angstrom level, as it can be used to characterise the thicknesses, roughnesses and compositions of both underlying metal films, their oxide layers and protective organic layers deposited at the surface. These can all be observed as a function of pH, temperature, pressure and/or electrical potential by the choice of the appropriate cell design.

Particular advantages of NR over other techniques include its significant scattering from light elements, including H and Li, and also its variation in scattering for different isotopes of the same element. It therefore allows detailed characterisation of even very thin adsorbed organic layers at buried interfaces that would be difficult to see using other methods. Furthermore, as illustrated by several of the papers outlined above, NR has provided a unique opportunity to view ingress of hydrogen, water and various ions through film layers and has hence been used to study the nature of passive oxide films in different conditions, as well as the ability of coatings to act as barriers against attacking corrosive species. Solvent contrast variation has been used both to provide extra datasets to improve the model fitting and, more importantly, to blank out some parts of each system and focus in on specific components. The entire corroding system can, therefore, be characterised in situ, component by component.

Challenges with NR include the necessity for very clean, very flat samples, as well as the need to apply for competitive beam time at international facilities. In addition, the long measurement times due to the relatively low neutron flux is non-ideal for some corrosion studies, although there do exist approaches to overcome this, as discussed above. Specular NR is also only able to give structural information in the plane perpendicular to the surface and so cannot distinguish between pit formation and laterally-averaged corrosion. Some off-specular studies have been made, but these are challenging to perform and interpret.

Despite these challenges, it is clear from the numerous examples presented above that there is great potential of NR to greatly improve fundamental understanding in the area of corrosion and corrosion inhibitors.

Acknowledgments: We thank the other authors in the field who have generously communicated recent or unpublished results for our discussion, those who have allowed us to reprint their figures and the University of Cambridge and BP Institute for supporting our work.

Conflicts of Interest: The authors declare no conflict of interest.

References

1. Noël, J.J. Oxide films and corrosion. In *Neutron Reflectometry—A Probe for Materials Surfaces*; International Atomic Energy Agency: Vienna, Austria, 2004; pp. 79–84.
2. Mills, A.; Hazafy, D. UV-activated photocatalyst films and inks for cleaning tarnished metals. *Chem. Commun.* **2012**, *48*, 525–527. [[CrossRef](#)] [[PubMed](#)]
3. Scully, J.C. *The Fundamentals of Corrosion*, 3rd ed.; Pergamon Press: Oxford, UK, 1990.
4. Schweitzer, P.A. *Corrosion Engineering Handbook*, 2nd ed.; Marcel Dekker, Inc.: New York, NY, USA, 1996.
5. Dariva, C.G.; Galio, A.F. Corrosion inhibitors-principles, mechanisms and applications. In *Developments in Corrosion Protection*; Aliofkhaezai, M., Ed.; InTech: West Palm Beach, FL, USA, 2014.
6. Anbarasi, C.M.; Rajendran, S.; Pandiarajan, M.; Krishnaveni, A. An encounter with corrosion inhibitors. *Eur. Chem. Bull.* **2013**, *2*, 197–207.
7. Nii, K. On the dissolution behaviour of NiO. *Corros. Sci.* **1970**, *10*, 571–583.

8. Khalifa, D.R.; Abdallah, S.M. Corrosion inhibition of some organic compounds on low carbon steel in hydrochloric acid solution. *Port. Electrochim. Acta* **2011**, *29*, 47–56. [[CrossRef](#)]
9. Kuznetsov, Y.I.; Mercer, A.D.; Thomas, J.G.N. *Organic Inhibitors of Corrosion of Metals*; Springer: New York, NY, USA, 1996.
10. Welbourn, R.J.L.; Truscott, C.L.; Skoda, M.W.A.; Zorbakhsh, A.; Clarke, S.M. Corrosion and inhibition of copper in hydrocarbon solution on a molecular level investigated using neutron reflectometry and XPS. *Corros. Sci.* **2017**, *115*, 68–77. [[CrossRef](#)]
11. Yilmazbayhan, A.; Motta, A.T.; Comstock, R.J.; Sabol, G.P.; Lai, B.; Cai, Z. Structure of zirconium alloy oxides formed in pure water studied with synchrotron radiation and optical microscopy: Relation to corrosion rate. *J. Nucl. Mater.* **2004**, *324*, 6–22. [[CrossRef](#)]
12. Kelly, R.G.; Scully, J.R.; Shoesmith, D.W.; Buchheit, R.G. *Electrochemical Techniques in Corrosion Science and Engineering*; Marcel Dekker, Inc.: New York, NY, USA, 2003.
13. Hayfield, P. Ellipsometry in corrosion technology. In *Advances in Corrosion Science and Technology*; Fontana, M.G., Staehle, R.W., Eds.; Springer: New York, NY, USA, 1972; pp. 43–113.
14. Takahashi, Y.; Matsubara, E.; Suzuki, S.; Okamoto, Y.; Komatsu, T.; Konishi, H.; Mizuki, J.; Waseda, Y. In-situ X-ray diffraction of corrosion products formed on iron surfaces. *Mater. Trans.* **2005**, *46*, 637–642. [[CrossRef](#)]
15. Lelièvre, G.; Fruchart, D.; Convert, P.; Lefèvre-Joud, F. Characterisation by neutron diffraction in high temperature pressurised water of the surface corrosion and hydrogen embrittlement of zircaloy-4. *J. Alloys Compd.* **2002**, *347*, 288–294. [[CrossRef](#)]
16. Kobe, B.A.; Ramamurthy, S.; Biesinger, M.C.; McIntyre, N.S.; Brennenstuhl, A.M. XPS imaging investigations of pitting corrosion mechanisms in Inconel 600. *Surf. Interface Anal.* **2005**, *37*, 478–494. [[CrossRef](#)]
17. Miller, K.L. Neutron Reflectivity of Aqueous Mineral and Metal Oxide Interfaces. Ph.D. Thesis, University of Cambridge, Cambridge, UK, 2014.
18. Sánchez, J.; Fulla, J.; Andrade, C.; Gaitero, J.J.; Porro, A. AFM study of the early corrosion of a high strength steel in a diluted sodium chloride solution. *Corros. Sci.* **2008**, *50*, 1820–1824. [[CrossRef](#)]
19. Morsch, S.; Lyon, S.; Smith, S.D.; Gibbon, S.R. Mapping water uptake in an epoxy-phenolic coating. *Prog. Org. Coat.* **2015**, *86*, 173–180. [[CrossRef](#)]
20. Speller, F.N.; Kendall, V.V. A new method of measuring corrosion in water. *Ind. Eng. Chem.* **1923**, *15*, 134–139. [[CrossRef](#)]
21. Amin, M.A. Weight loss, polarisation, electrochemical impedance spectroscopy, SEM and EDX studies of the corrosion inhibition of copper in aerated NaCl solutions. *J. Appl. Electrochem.* **2006**, *36*, 215–226. [[CrossRef](#)]
22. Lützenkirchen-Hecht, D.; Strehlow, H.-H. Synchrotron methods for corrosion research. In *Analytical Methods in Corrosion Science and Engineering*; Marcus, P., Mansfeld, F.B., Eds.; CRC Press: New York, NY, USA, 2005; pp. 169–236.
23. Chung, S.C.; Lin, A.S.; Chang, J.R.; Shih, H.C. EXAFS study of atmospheric corrosion products on zinc at the initial stage. *Corros. Sci.* **2000**, *42*, 1599–1610. [[CrossRef](#)]
24. Lima, E.; Bosch, P.; Lara, V.; Villarreal, E.; Piña, C.; Torres, G.; Martín, S.; León, B. Metal corrosion in bones implanted with Zinalco—A SAXS and NMR study. *J. Biomed. Mater. Res. B* **2006**, *76*, 203–210. [[CrossRef](#)] [[PubMed](#)]
25. Song, C.H.; Choi, Y.; Shin, E.H.; Seong, B.S.; Han, Y.S. Analysis of organic-coated steels by using small-angle neutron scattering. *Phys. Met. Metallogr.* **2014**, *115*, 1333–1337. [[CrossRef](#)]
26. Penfold, J. Principles of reflectometry with reactors and pulsed sources. In *Neutron Reflectometry—A Probe for Materials Surfaces*; International Atomic Energy Agency: Vienna, Austria, 2004; pp. 29–44.
27. Penfold, J.; Thomas, R.K. The application of the specular reflection of neutrons to the study of surfaces and interfaces. *J. Phys. Condens. Mater.* **1990**, *2*, 1369–1412. [[CrossRef](#)]
28. Lu, J.R.; Marrocco, A.; Su, T.J.; Thomas, R.K.; Penfold, J. Adsorption of dodecyl sulfate surfactants with monovalent metal counterions at the air-water interface studied by neutron reflection and surface tension. *J. Colloid Interface Sci.* **1993**, *158*, 303–316. [[CrossRef](#)]
29. Li, Z.X.; Dong, C.C.; Thomas, R.K. Neutron reflectivity studies of the surface excess of gemini surfactants at the air-water interface. *Langmuir* **1999**, *15*, 4392–4396. [[CrossRef](#)]
30. Eastoe, J.; Dalton, J.S. Dynamic surface tension and adsorption mechanisms of surfactants at the air-water interface. *Adv. Colloid Interface. Sci.* **2000**, *85*, 103–144. [[CrossRef](#)]

31. Browning, K.L.; Griffin, L.R.; Gutfreund, P.; Barker, R.D.; Clifton, L.A.; Hughes, A.; Clarke, S.M. Specular neutron reflection at the mica/water interface-irreversible adsorption of a cationic dichain surfactant. *J. Appl. Cryst.* **2014**, *47*, 1638–1646. [[CrossRef](#)]
32. Stocker, I.N.; Miller, K.L.; Lee, S.Y.; Welbourn, R.J.L.; Mannion, A.R.; Collins, I.R.; Webb, K.J.; Wildes, A.; Kinane, C.J.; Clarke, S.M. Neutron reflection at the calcite-water interface. *Prog. Colloid Polym. Sci.* **2012**, *139*, 91–99.
33. Sferrazza, M.; Jones, R.A.L.; Penfold, J.; Bucknall, D.B.; Webster, J.R.P. Neutron reflectivity studies of the structure of polymer/polymer and polymer/substrate interfaces at the nanometer level. *J. Mater. Chem.* **2000**, *10*, 127–132. [[CrossRef](#)]
34. Speranza, F.; Pilkington, G.A.; Dane, T.G.; Cresswell, P.T.; Li, P.; Jacobs, R.M.J.; Arnold, T.; Bouchenoire, L.; Thomas, R.K.; Briscoe, W.H. Quiescent bilayers at the mica-water interface. *Soft Matter* **2013**, *9*, 7028–7041. [[CrossRef](#)]
35. Griffin, L.R.; Browning, K.L.; Truscott, C.L.; Clifton, L.A.; Clarke, S.M. Complete bilayer adsorption of C₁₆TAB on the surface of mica using neutron reflection. *J. Phys. Chem. B* **2015**, *119*, 6457–6461. [[CrossRef](#)] [[PubMed](#)]
36. Kreuzer, M.; Kaltofen, T.; Steitz, R.; Zehnder, B.H.; Dahint, R. Pressure cell for investigations of solid-liquid interfaces by neutron reflectivity. *Rev. Sci. Instrum.* **2011**, *82*, 023902. [[CrossRef](#)] [[PubMed](#)]
37. Jeworrek, C.; Steitz, R.; Czeslik, C.; Winter, R. High pressure cell for neutron reflectivity measurements up to 2500 bar. *Rev. Sci. Instrum.* **2011**, *82*, 025106. [[CrossRef](#)] [[PubMed](#)]
38. Carmichael, J.R.; Rother, G.; Browning, J.F.; Ankner, J.F.; Banuelos, J.L.; Anovitz, L.M.; Wesolowski, D.J.; Cole, D.R. High-pressure cell for neutron reflectometry of supercritical and subcritical fluids at solid interfaces. *Rev. Sci. Instrum.* **2012**, *83*, 045108. [[CrossRef](#)] [[PubMed](#)]
39. Welbourn, R.J.L. Adsorbed Layers under Challenging Conditions at the Solid-Liquid Interface. Ph.D. Thesis, University of Cambridge, Cambridge, UK, 2016.
40. Baker, S.M.; Smith, G.; Pynn, R.; Butler, P.; Hayter, J.; Hamilton, W.; Magid, L. Shear cell for the study of liquid-solid interfaces by neutron scattering. *Rev. Sci. Instrum.* **1994**, *65*, 412–416. [[CrossRef](#)]
41. Tun, Z.; Noël, J.J.; Shoesmith, D.W. Electrochemical modifications on the surface of a Ti film. *Physica B* **1998**, *241–243*, 1107–1109. [[CrossRef](#)]
42. Burgess, I.; Zamlynny, V.; Szymanski, G.; Schwan, A.L.; Faragher, R.J.; Lipkowski, J.; Majewski, J.; Satija, S. Neutron reflectivity studies of field driven transformations in a monolayer of 4-pentadecyl pyridine at Au electrode surfaces. *J. Electroanal. Chem.* **2003**, *550–551*, 187–199. [[CrossRef](#)]
43. Zamlynny, V.; Burgess, I.; Szymanski, G.; Lipkowski, J.; Majewski, J.; Smith, G.; Satija, S.; Ivkov, R. Electrochemical and neutron reflectivity studies of spontaneously formed amphiphilic surfactant bilayers at the gold-solution interface. *Langmuir* **2000**, *16*, 9861–9870. [[CrossRef](#)]
44. Burgess, I.; Li, M.; Horswell, S.L.; Szymanski, G.; Lipkowski, J.; Majewski, J.; Satija, S. Electric field-driven transformations of a supported model biological membrane—An electrochemical and neutron reflectivity study. *Biophys. J.* **2004**, *86*, 1763–1776. [[CrossRef](#)]
45. Richardson, R.M.; Swann, M.J.; Hillman, A.R.; Roser, S.J. In situ neutron reflectivity studies of electroactive films. *Faraday Discuss.* **1992**, *94*, 295–306. [[CrossRef](#)]
46. Demkowicz, M.J.; Majewski, J.; Liss, K.-D. Probing interfaces in metals using neutron reflectometry. *Metals* **2016**, *6*, 20–37. [[CrossRef](#)]
47. Felici, R.; Penfold, J.; Ward, R.C.; Williams, W.G. A polarised neutron reflectometer for studying surface magnetism. *Appl. Phys. A* **1988**, *45*, 169–174. [[CrossRef](#)]
48. Jones, R.A.L.; Fletcher, P.; Thomas, R.K.; Roser, S.; Dickinson, E.; Bucknall, D.G.; Penfold, J.; Webster, J.R.P.; Zarbakhsh, A.; Richardson, R.M.; et al. *ICANS-SII and ESS-PM4*; Bercher, R., Ed.; Paul Scherrer Institute: Villigen, Switzerland, 1995; p. 440.
49. Webster, J.; Holt, S.; Dalgliesh, R. INTER: The chemical interfaces reflectometer on target station 2 at ISIS. *Physica B* **2006**, *385–386*, 1164–1166. [[CrossRef](#)]
50. Charlton, T.R.; Coleman, R.L.S.; Dalgliesh, R.M.; Kinane, C.J.; Neylon, C.; Langridge, S.; Plomp, J.; Webb, N.G.J.; Webster, J.R.P. Advances in neutron reflectometry at ISIS. *Neutron News* **2011**, *22*, 15–18. [[CrossRef](#)]
51. Cubitt, R.; Fragneto, G. D17: The new reflectometer at the ILL. *Appl. Phys. A* **2002**, *74*, S329–S331. [[CrossRef](#)]

52. Campbell, R.A.; Wacklin, H.P.; Sutton, I.; Cubitt, R.; Fragneto, G. FIGARO: The new horizontal neutron reflectometer at the ILL. *Eur. Phys. J. Phys.* **2011**, *126*, 107–129. [[CrossRef](#)]
53. Paul, A.; Krist, T.; Teichert, A.; Steitz, R. Specular and off-specular scattering with polarisation and polarisation analysis on reflectometer V6 at BER II, HZB. *Physica B* **2011**, *406*, 1598–1606. [[CrossRef](#)]
54. Gupta, M.; Gutberlet, T.; Stahn, J.; Keller, P.; Clemens, D. AMOR—The time-of-flight neutron reflectometer at SINQ/PSI. *Pramana-J. Phys.* **2004**, *63*, 57–63. [[CrossRef](#)]
55. Pan, G.; Yim, H.; Kent, M.S.; Majewski, J.; Schaefer, D.W. Neutron reflectivity investigation of bis-amino silane films. *J. Adhes. Sci. Technol.* **2003**, *17*, 2175–2189. [[CrossRef](#)]
56. Griffin, L.R.; Browning, K.L.; Clarke, S.M.; Smith, A.M.; Perkin, S.; Skoda, M.W.A.; Norman, S.E. Direct measurements of ionic liquid layering at a single mica-liquid interface and in nano-films between two mica-liquid interfaces. *Phys. Chem. Chem. Phys.* **2017**, *19*, 297–304. [[CrossRef](#)] [[PubMed](#)]
57. Griffin, L.R.; Browning, K.L.; Lee, S.Y.; Skoda, M.W.A.; Rogers, S.E.; Clarke, S.M. Multilayering of calcium aerosol-OT at the mica/water interface studied with neutron reflection: Formation of a condensed lamellar phase at the CMC. *Langmuir* **2016**, *32*, 13054–13064. [[CrossRef](#)] [[PubMed](#)]
58. Nelson, A. Co-refinement of multiple-contrast neutron/X-ray reflectivity data using MOTOFIT. *J. Appl. Cryst.* **2006**, *39*, 273–276. [[CrossRef](#)]
59. Björck, M.; Andersson, G. GenX: An extensible X-ray reflectivity refinement program utilising differential evolution. *J. Appl. Cryst.* **2007**, *40*, 1174–1178. [[CrossRef](#)]
60. Majkrzak, C.F.; Berk, N.F. Exact determination of the phase in neutron reflectometry. *Phys. Rev. B* **1995**, *52*, 10827–10830. [[CrossRef](#)]
61. Bowers, J.; Zorbakhsh, A.; Webster, J.R.P.; Hutchings, L.R.; Richards, R.W. Neutron reflectivity studies at liquid-liquid interfaces: Methodology and analysis. *Langmuir* **2001**, *17*, 140–145. [[CrossRef](#)]
62. Zorbakhsh, A.; Querol, A.; Bowers, J.; Yaseen, M.; Lu, J.R.; Webster, J.R.P. Neutron reflection from the liquid-liquid interface: Adsorption of hexadecylphosphorylcholine to the hexadecane-aqueous solution interface. *Langmuir* **2005**, *21*, 11704–11709. [[CrossRef](#)] [[PubMed](#)]
63. Wildes, A.R. *Neutron Reflectometry—A Probe for Materials Surfaces*; International Atomic Energy Agency: Vienna, Austria, 2004; pp. 145–160.
64. Ankner, J.F.; Felcher, G.P. Polarised-neutron reflectometry. *J. Magn. Magn. Mater.* **1999**, *200*, 741–754. [[CrossRef](#)]
65. Wood, M.H.; Welbourn, R.J.L.; Charlton, T.; Zorbakhsh, A.; Casford, M.T.; Clarke, S.M. Hexadecylamine adsorption at the iron oxide-oil interface. *Langmuir* **2013**, *29*, 13735–13742. [[CrossRef](#)] [[PubMed](#)]
66. Rennie, A.R. Neutron reflection studies of solid/liquid interfaces. In *Neutron Reflectometry—A Probe for Materials Surfaces*; International Atomic Energy Agency: Vienna, Austria, 2004; pp. 85–94.
67. Dong, X.; Argekar, S.; Wang, P.; Schaefer, D.W. In situ evolution of trivalent chromium process passive film on Al in a corrosive aqueous environment. *Appl. Mater. Int.* **2011**, *3*, 4206–4214. [[CrossRef](#)] [[PubMed](#)]
68. Tun, Z.; Noël, J.J.; Shoesmith, D.W. Electrochemical modification of the passive oxide layer on a Ti film observed by in situ neutron reflectometry. *J. Electrochem. Soc.* **1999**, *146*, 988–994. [[CrossRef](#)]
69. Helling, M.S.; Rennie, A.R.; Hughes, A.V. Effect of concentration and addition of ions on the adsorption of aerosol-OT to sapphire. *Langmuir* **2010**, *26*, 14567–14573. [[CrossRef](#)] [[PubMed](#)]
70. Helling, M.S.; Rennie, A.R.; Hughes, A.V. Adsorption of aerosol-OT to sapphire: Lamellar structures studied with neutrons. *Langmuir* **2011**, *27*, 4669–4678. [[CrossRef](#)] [[PubMed](#)]
71. Welbourn, R.J.L.; Lee, S.Y.; Gutfreund, P.; Hughes, A.; Zorbakhsh, A.; Clarke, S.M. Neutron reflection study of the adsorption of the phosphate surfactant NaDEHP onto alumina from water. *Langmuir* **2015**, *31*, 3377–3384. [[CrossRef](#)] [[PubMed](#)]
72. Lee, S.Y.; Welbourn, R.; Clarke, S.M.; Skoda, M.W.A.; Clifton, L.; Zorbakhsh, A. Adsorption of sodium hexanoate on α -alumina. *J. Colloid Int. Sci.* **2013**, *407*, 348–353. [[CrossRef](#)] [[PubMed](#)]
73. Campana, M.; Teichert, A.; Clarke, S.; Steitz, R.; Webster, J.R.P.; Zorbakhsh, A. Surfactant adsorption at the metal-oil interface. *Langmuir* **2011**, *27*, 6085–6090. [[CrossRef](#)] [[PubMed](#)]
74. Wood, M.H.; Casford, M.T.; Steitz, R.; Zorbakhsh, A.; Welbourn, R.J.L.; Clarke, S.M. Comparative adsorption of saturated and unsaturated fatty acids at the iron oxide/oil interface. *Langmuir* **2016**, *32*, 534–540. [[CrossRef](#)] [[PubMed](#)]
75. Wood, M.H.; Welbourn, R.J.L.; Zorbakhsh, A.; Gutfreund, P.; Clarke, S.M. Polarised neutron reflectometry of nickel corrosion inhibitors. *Langmuir* **2015**, *31*, 7062–7072. [[CrossRef](#)] [[PubMed](#)]

76. Wood, M.H.; Browning, K.L.; Barker, R.D.; Clarke, S.M. Using neutron reflectometry to discern the structure of fibrinogen adsorption at the stainless steel/aqueous interface. *J. Phys. Chem. B* **2016**, *120*, 5405–5416. [[CrossRef](#)] [[PubMed](#)]
77. Noël, J.J.; Shoesmith, D.W.; Tun, Z. Anodic oxide growth and hydrogen absorption on Zr in neutral aqueous solution: A comparison to Ti. *J. Electrochem. Soc.* **2008**, *155*, C444–C454. [[CrossRef](#)]
78. Mitchell, W.J.; Burn, P.L.; Thomas, R.K.; Fragneto, G. Probing the polymer-electrode interface using neutron reflection. *Appl. Phys. Lett.* **2003**, *82*, 2724–2726. [[CrossRef](#)]
79. Noël, J.J.; Jensen, H.L.; Tun, Z.; Shoesmith, D.W. Electrochemical modification of the passive oxide layer on Zr-2.5Nb observed by in situ neutron reflectometry. *Electrochem. Solid State Lett.* **2000**, *3*, 473–476. [[CrossRef](#)]
80. Rieker, T.; Hubbard, P.; Majewski, J.; Smith, G.; Moody, N. Neutron reflectivity investigation of the effects of harsh environments on Ta₂N thin films. *Thin Solid Films* **1999**, *346*, 116–119. [[CrossRef](#)]
81. Kalisvaart, P.; Lubber, E.; Fritzsche, H.; Mitlin, D. Effect of alloying magnesium with chromium and vanadium on hydrogenation kinetics studied with neutron reflectometry. *Chem. Commun.* **2011**, *47*, 4294–4296. [[CrossRef](#)] [[PubMed](#)]
82. Watkins, E.B.; Majewski, J.; Baldwin, J.K.; Chen, Y.; Li, N.; Hoagland, R.G.; Yadav, S.K.; Liu, X.Y.; Beyerlein, I.J.; Mara, N.A. Neutron reflectometry investigations of interfacial structures of Ti/TiN layers deposited by magnetron sputtering. *Thin Solid Films* **2016**, *616*, 399–407. [[CrossRef](#)]
83. Mayes, M.A.; Jagadamma, S.; Ambaye, H.; Petridis, L.; Lauter, V. Neutron reflectometry reveals the internal structure of organic compounds deposited on aluminium oxide. *Geoderma* **2013**, 182–188. [[CrossRef](#)]
84. Owejan, J.E.; Owejan, J.P.; DeCaluwe, S.C.; Dura, J.A. Solid electrolyte interphase in Li-ion batteries: Evolving structures measured in situ by neutron reflectometry. *Chem. Mater.* **2012**, *24*, 2133–2140. [[CrossRef](#)]
85. Li, N.; Thomas, R.K.; Rennie, A.R. Adsorption of non-ionic surfactants to the sapphire/solution interface-effects of temperature and pH. *J. Colloid Int. Sci.* **2012**, *369*, 287–293. [[CrossRef](#)] [[PubMed](#)]
86. Li, N.N.; Thomas, R.K.; Rennie, A.R. Neutron reflectometry of anionic surfactants on sapphire: A strong maximum in the adsorption near the critical micelle concentration. *J. Colloid Int. Sci.* **2016**, *471*, 81–88. [[CrossRef](#)] [[PubMed](#)]
87. Junghans, A.; Chellappa, R.; Wang, P.; Majewski, J.; Luciano, G.; Marcelli, R.; Proietti, E. Neutron reflectometry studies of aluminium-saline water interface under hydrostatic pressure. *Corros. Sci.* **2015**, *90*, 101–106. [[CrossRef](#)]
88. Wang, P.; Dong, X.; Schaefer, D.W. Structure and water-barrier properties of vanadate-based corrosion inhibitor films. *Corros. Sci.* **2010**, *52*, 943–949. [[CrossRef](#)]
89. Hu, N.; Dong, X.; He, X.; Browning, J.F.; Schaefer, D.W. Effect of sealing on the morphology of anodised aluminium oxide. *Corros. Sci.* **2015**, *97*, 17–24. [[CrossRef](#)]
90. Armstrong, N.R.; Quinn, R.K. Auger and X-ray photoelectron spectroscopic and electrochemical characterisation of titanium thin film electrodes. *Surf. Sci.* **1977**, *67*, 451–468. [[CrossRef](#)]
91. Wiesler, D.G.; Majkrzak, C.F. Neutron reflectometry studies of surface oxidation. *Physica B* **1994**, *198*, 181–186. [[CrossRef](#)]
92. Wiesler, D.G.; Majkrzak, C.F. Growth and dissolution of protective oxide films on titanium: An in situ neutron reflectivity study. *Manag. Res. Soc. Symp. Proc.* **1995**, *376*, 247–257. [[CrossRef](#)]
93. Noël, J.J.; Smith, J.M.; Vezvaie, M.; Tun, Z. In Situ Neutron Reflectometry Study of Hydrogen Absorption By Zirconium during Cathodic Polarization. In Proceedings of the 19th Pacific Basin Nuclear Conference, Vancouver, BC, Canada, 24–28 August 2014; p. 2821.
94. Singh, S.; Basu, S.; Gupta, M.; Majkrzak, C.F.; Kienzle, P.A. Growth kinetics of intermetallic alloy phase at the interfaces of a Ni/Al multilayer using polarised neutron and X-ray reflectometry. *Phys. Rev. B* **2010**, *81*, 235413. [[CrossRef](#)]
95. Singh, S.; Poswal, A.K.K.; Ghosh, S.K.K.; Basu, S. Scattering length density profile of Ni film under controlled corrosion: A study in neutron reflectometry. *Pramana J. Phys.* **2008**, *71*, 1097–1101. [[CrossRef](#)]
96. Singh, S.; Basu, S. Microscopic characterisation of corrosion morphology: A study in specular and diffuse neutron reflectivity. *Surf. Sci.* **2006**, *600*, 493–496. [[CrossRef](#)]
97. Singh, S.; Basu, S.; Poswal, A.K.K.; Tokas, R.B.B.; Ghosh, S.K.K. Electrochemically controlled pitting corrosion in Ni film: A study of AFM and neutron reflectometry. *Corros. Sci.* **2009**, *51*, 575–580. [[CrossRef](#)]

98. Morales-Gil, P.; Walczak, M.S.; Cottis, R.A.; Romero, J.M.; Lindsay, R. Corrosion inhibitor binding in an acidic medium: Interaction of 2-mercaptobenzimidazole with carbon-steel in hydrochloric acid. *Corros. Sci.* **2014**, *85*, 109–114. [[CrossRef](#)]
99. Molchan, I.S.; Thompson, G.E.; Lindsay, R.; Skeldon, P.; Likodimos, V.; Romanos, G.E.; Falaras, P.; Adamova, G.; Iliev, B.; Schubert, T.J.S. Corrosion behaviour of mild steel in 1-alkyl-3-methylimidazolium tricyanomethanide ionic liquids for CO₂ capture applications. *RSC Adv.* **2014**, *4*, 5300–5311. [[CrossRef](#)]
100. Saville, P.M.; Gonsalves, M.; Hillman, A.R.; Cubitt, R. Dynamic neutron reflectivity measurements during redox switching of nickel hydroxide films. *J. Phys. Chem. B* **1997**, *101*, 1–4. [[CrossRef](#)]
101. Metelev, S.V.; Pleshanov, N.K.; Menelle, A.; Pusenkov, V.M.; Schebetov, A.F.; Soroko, Z.N.; Ul'yanov, V.A. The study of oxidation of thin metal films by neutron reflectometry. *Physica B* **2001**, *297*, 122–125. [[CrossRef](#)]
102. Campana, M. Structural Studies of Surfactants at Interfaces. Ph.D. Thesis, University of London, London, UK, 2012.
103. Wood, M.H. Adsorption at the Solid/Liquid Interface. Ph.D. Thesis, University of Cambridge, Cambridge, UK, 2015.
104. Kruger, J.; Krebs, L.A.; Long, G.G.; Anker, J.F.; Majkrzak, C.F. Passivity of metals and alloys and its breakdown—New results from new non-electrochemical techniques. *Mater. Sci. Forum* **1995**, *185–188*, 367–376. [[CrossRef](#)]
105. Feng, J. Characterization of Native Oxide and Passive Film on Iron and Iron-Chromium Alloy. Ph.D. Thesis, University of Cincinnati, Cincinnati, OH, USA, 2014.
106. Wood, M.H.; Wood, T.J.; Poon, J.; Welbourn, R.J.L.; Madden, D.; Clarke, S.M. An X-ray and neutron reflectometry study of iron corrosion in seawater at the angstrom level. 2017; in preparation.
107. Jerliu, B.; Hüger, E.; Dörrer, L.; Seidlhofer, B.K.; Steitz, R.; Oberst, V.; Geckle, U.; Bruns, M.; Schmidt, H. Volume expansion during lithiation of amorphous silicon thin film electrodes studied by in-operando neutron reflectometry. *J. Phys. Chem. C* **2014**, *118*, 9395–9399. [[CrossRef](#)]
108. Jerliu, B.; Dörrer, L.; Hüger, E.; Borchardt, G.; Steitz, R.; Geckle, U.; Oberst, V.; Bruns, M.; Schneider, O.; Schmidt, H. Neutron reflectometry studies of the lithiation of amorphous silicon electrodes in lithium-ion batteries. *Phys. Chem. Chem. Phys.* **2013**, *15*, 7777–7784. [[CrossRef](#)] [[PubMed](#)]
109. Wagemaker, M.; Van de Krol, R.; Van Well, A.A. Nano-morphology of lithiated thin film TiO₂ anatase probed with in situ neutron reflectometry. *Physica B* **2003**, *336*, 124–129. [[CrossRef](#)]
110. Hirayama, M.; Yonemura, M.; Suzuki, K.; Torikai, N.; Smith, H.; Watkinsand, E.; Majewski, J.; Kanno, R. Surface characterisation of LiFePO₄ epitaxial thin films by X-ray/neutron reflectometry. *Electrochemistry* **2010**, *78*, 413–415. [[CrossRef](#)]
111. Browning, J.F.; Baggetto, L.; Jungjohann, K.L.; Wang, Y.; Tenhaeff, W.E.; Keum, J.K.; Wood, D.L.; Veith, G.M. In situ determination of the liquid/solid interface thickness and composition for the Li ion cathode LiMn_{1.5}Ni_{0.5}O₄. *Appl. Mater. Int.* **2014**, *6*, 18569–18576. [[CrossRef](#)] [[PubMed](#)]
112. Cooper, J.M.; Cubitt, R.; Dalglish, R.M.; Gadegaard, N.; Glidle, A.; Hillman, A.R.; Mortimer, R.J.; Ryder, K.S.; Smith, E.L. Dynamic in situ electrochemical neutron reflectivity measurements. *J. Am. Chem. Soc.* **2004**, *126*, 15362–15363. [[CrossRef](#)] [[PubMed](#)]
113. Wilson, R.W.; Bailey, L.; Cubitt, R.; Gonsalves, M.; Glidle, A.; Hillman, A.R.; Vos, J.G.; Hogan, C.; Webster, J.R.P. A study of [Os(bipy)₂(PVP)_{3.3}(PS)_{6.7}Cl]⁺ polymer film modified electrodes using neutron reflectivity. *Phys. Chem. Chem. Phys.* **1999**, *1*, 843–853. [[CrossRef](#)]
114. Glidle, A.; Hillman, A.R.; Ryder, K.S.; Smith, E.L.; Cooper, J.; Gadegaard, N.; Webster, J.R.P.; Dalglish, R.; Cubitt, R. Use of neutron reflectivity to measure the dynamics of solvation and structural changes in polyvinylferrocene films during electrochemically controlled redox cycling. *Langmuir* **2009**, *25*, 4093–4103. [[CrossRef](#)] [[PubMed](#)]
115. Lauw, Y.; Horne, M.D.; Rodopoulos, T.; Lockett, V.; Akgun, B.; Hamilton, W.A.; Nelson, A.R. Structure of [C₄mpyr][NTf₂] room-temperature ionic liquid at charged gold interfaces. *Langmuir* **2012**, *28*, 7374–7381. [[CrossRef](#)] [[PubMed](#)]
116. Lauw, Y.; Rodopoulos, T.; Gross, M.; Nelson, A.; Gardner, R.; Horne, M.D. Electrochemical cell for neutron reflectometry studies of the structure of ionic liquids at electrified interface. *Rev. Sci. Instrum.* **2010**, *81*, 074101. [[CrossRef](#)] [[PubMed](#)]
117. Itkis, D.M.; Velasco-Velez, J.J.; Knop-Gericke, A.; Vyalikh, A.; Avdeev, M.V.; Yashina, L.V. Probing operating electrochemical interfaces by photons and neutrons. *ChemElectroChem* **2015**, *2*, 1427–1445. [[CrossRef](#)]

118. Wilson, R.W.; Cubitt, R.; Glidle, A.; Hillman, A.R.; Saville, P.M.; Vos, J.G. A neutron reflectivity study of $[\text{Os}(\text{bipy})_2(\text{PVP})_{10}\text{Cl}]^+$ polymer film modified electrodes: Effect of pH and counterion. *J. Electrochem. Soc.* **1998**, *145*, 1454–1461. [[CrossRef](#)]
119. Glidle, A.; Hadyoon, C.S.; Gadegaard, N.; Cooper, J.M.; Hillman, A.R.; Wilson, R.W.; Ryder, K.S.; Webster, J.R.P.; Cubitt, R. Evaluating the influence of deposition conditions on solvation of reactive conducting polymers with neutron reflectivity. *J. Phys. Chem. B* **2005**, *109*, 14335–14343. [[CrossRef](#)] [[PubMed](#)]
120. Glidle, A.; Pearson, P.E.; Smith, E.L.; Cooper, J.M.; Cubitt, R.; Dalgliesh, R.M.; Hillman, A.R.; Ryder, K.S. Determining compositional profiles within conducting polymer films following reaction with vapour phase reagents. *J. Phys. Chem. B* **2007**, *111*, 4043–4053. [[CrossRef](#)] [[PubMed](#)]
121. Wang, Y.; Watkins, E.; Ilavsky, J.; Metroke, T.L.; Wang, P.; Lee, B.; Schaefer, D.W. Water-barrier properties of mixed bis [trimethoxysilylpropyl] amine and vinyltriacetoxysilane films. *J. Phys. Chem. B* **2007**, *111*, 7041–7051. [[CrossRef](#)] [[PubMed](#)]
122. Yim, H.; Kent, M.S.; Tallant, D.R.; Garcia, M.J.; Majewski, J. Hygrothermal Degradation of (3-glycidoxypropyl) trimethoxysilane films studied by neutron and X-ray reflectivity and attenuated total reflection infrared spectroscopy. *Langmuir* **2005**, *21*, 4382–4392. [[CrossRef](#)] [[PubMed](#)]
123. Pan, G.; Watkins, E.; Majewski, J.; Schaefer, D.W. Effect of thickness on the water-barrier properties of silane films. *J. Phys. Chem. C* **2007**, *111*, 15325–15330. [[CrossRef](#)]
124. Payra, D.; Naito, M.; Fujii, Y.; Yamada, N.L.; Hiromoto, S.; Singh, A. Bioinspired adhesive polymer coatings for efficient and versatile corrosion resistance. *RSC Adv.* **2015**, *5*, 15977–159834. [[CrossRef](#)]
125. Wang, Y.; Wang, P.; Kohls, D.; Hamilton, W.A.; Schaefer, D.W. Water absorption and transport in bis-silane films. *Phys. Chem. Chem. Phys.* **2009**, *11*, 161–166. [[CrossRef](#)] [[PubMed](#)]
126. Wang, P.; Schaefer, D.W. Salt exclusion in silane-laced epoxy coatings. *Langmuir* **2010**, *26*, 234–240. [[CrossRef](#)] [[PubMed](#)]
127. Pan, G.; Schaefer, D.W. Morphology and water-barrier properties of silane films on aluminium and silicon. *Thin Solid Films* **2006**, *503*, 259–267. [[CrossRef](#)]
128. Yim, H.; Kent, M.S.; Hall, J.S.; Benkoski, J.J.; Kramer, E.J. Probing the structure of organosilane films by solvent swelling and neutron and X-ray reflection. *J. Phys. Chem. B* **2002**, *106*, 2474–2481. [[CrossRef](#)]
129. Lechenault, F.; Rountree, C.L.; Cousin, F.; Bouchaud, J.P.; Ponson, L.; Bouchaud, E. Damage of silicate glasses during stress corrosion. *J. Phys. Conf. Ser.* **2011**, *319*, 012005. [[CrossRef](#)]
130. Barkhudarov, P.M.; Shah, P.B.; Watkins, E.B.; Doshi, D.A.; Brinker, C.J.; Majewski, J. Corrosion inhibition using superhydrophobic films. *Corros. Sci.* **2008**, *50*, 897–9902. [[CrossRef](#)]



© 2017 by the authors. Licensee MDPI, Basel, Switzerland. This article is an open access article distributed under the terms and conditions of the Creative Commons Attribution (CC BY) license (<http://creativecommons.org/licenses/by/4.0/>).